Genome Medicine

RESEARCH

Open Access

A comprehensive long-read sequencing system to assess DNA methylation at differentially methylated regions and imprinting-disorder-related genes

Tatsuki Urakawa[1,2], Atsushi Hattori[1,3], Yasuko Ogiwara[1], Hayate Masubuchi[1], Mizuho Igarashi[1], Sayuri Nakamura[1,4], Kaori Hara-Isono[1], Keisuke Ishiwata[5], Hiroko Ogata-Kawata[5], Hiromi Kamura[5], Yoko Kuroki[3,6,7], Kazuhiko Nakabayashi[5], Maki Fukami[1,3] and Masayo Kagami[1*]

Abstract

Background Imprinted genes are expressed in a parental-origin–specific manner. The imprinted regions including imprinted genes have differentially methylated regions (DMRs) with different 5-methylcytosine (5mC) patterns for CpGs on each parental allele, and DMRs function as imprinting control centers. Aberrant expression of the imprinted genes caused by structural variants involving DMRs, single-nucleotide variants in imprinted genes, uniparental disomy, and epimutation lead to imprinting disorders (IDs). Nanopore-based targeted long-read sequencing (T-LRS) can obtain sequence reads 10–100 kb long together with information on DNA methylation in each CpG and is cost-effective compared to whole-genome LRS. T-LRS is a valuable tool for efficient genetic testing for IDs and has great potential to elucidate the regulatory mechanisms in the imprinted regions. However, there is no T-LRS system targeting all ID-related regions.

Methods We conducted T-LRS targeting 78 DMRs and 22 genes in peripheral blood leukocytes from six healthy controls and set the normal range of methylation index (MI) for each CpG within the DMRs. To clarify the properties of DMRs, we compared MIs in CpGs within DMRs between haplotypes in 78 DMRs. To evaluate the usefulness of T-LRS, we conducted T-LRS on two previously reported patients with multi-locus imprinting disturbance (MLID) having pathogenic variants in MLID-causative genes and compared the MIs in CpGs within DMRs with those measured by array-based methylation analysis.

Results The median number of reads with 5mC and unmethylated cytosine in all DMRs in the six controls was over 40. We defined the normal range of MI for all CpGs in each allele and the total, and classified 78 DMRs into three categories, namely, 33 Complete-DMRs, 25 Partial-DMRs, and 20 Non-DMRs, based on the average of six controls for the median of differences of MIs in CpGs between haplotypes. We confirmed by T-LRS pathogenic variants in MLID-causative genes in patients with MLID. The patients' methylation defect patterns in T-LRS were similar to those in array-based methylation analysis, although T-LRS showed additional aberrantly methylated DMRs.

*Correspondence:
Masayo Kagami
kagami-ms@ncchd.go.jp
Full list of author information is available at the end of the article

Conclusions We established a T-LRS system targeting all ID-related regions, defined standard MI ranges in CpGs on each parental allele, and demonstrated the usefulness of T-LRS.

Keywords Long-read sequencing, Differentially methylated region, Adaptive sampling, Imprinting disorders, Methylation

Background

Imprinted genes are expressed in a parental-origin–specific manner. Differentially methylated regions (DMRs) in the imprinted region have different DNA methylation patterns for the fifth position of the cytosine residue (5-methylcytosine, 5mC) in CpGs on each parental allele and function as imprinting control centers for the imprinted genes [1, 2]. Sex-specific DNA methylation imprint in the DMRs is established in the parental gametes and fertilized egg and protected by maternal and fetal factors from genome-wide demethylation following fertilization [3]. The subcortical maternal complex (SCMC), consisting of NLRP2, NLRP5, NLRP7, PADI6, KHDC3L, OOEP, and TLE6, is expressed in oocytes and embryo up to the 16-cell stage and functions for maintenance of methylation of the DMRs as a maternal factor [2]; ZFP57 and ZNF445 play a role in maintaining the DNA methylation of the DMRs in the embryo after the 16-cell stage as fetal factors.

Abnormal expression of the imprinted genes results in imprinting disorders (IDs). The etiologies of IDs consist of uniparental disomy (UPD) of chromosomes containing the imprinted regions, structural variants (SVs) involving DMRs and/or imprinted genes, epimutation, and single-nucleotide variants (SNVs) in the disease-responsible imprinted genes. As shown in Table 1, the eight major IDs with associated disease names have multiple etiologies [2, 4–8]. The progress of molecular analysis has revealed multi-locus imprinting disturbance (MLID) with methylation defects in multiple-DMRs, and deleterious variants have been identified in *ZFP57* and *ZNF445* in patients with MLID, as well as in genes encoding proteins that constitute SCMC in their mothers [7, 8]. In addition, rare genetic causes for developing IDs, such as SNVs at the OCT4/SOX2 binding site within the *H19/IGF2*:intergenic (IG)-DMR (*H19*-DMR) on the maternal 11p15 imprinted region in cases with Beckwith-Wiedemann syndrome and retrotransposon insertion into the *GNAS* imprinted region in familial cases with pseudohypoparathyroidism type 1B (PHP1B), have been reported [2].

Because etiologies of IDs other than SNVs in the disease-responsible imprinted genes have aberrant methylation of the DMRs, methylation analysis for the DMRs is useful for screening examinations for IDs. Currently, methylation-specific multiple ligation-dependent probe amplification (MS-MLPA), which can simultaneously analyze the copy number and methylation status for the DMRs, is commonly used as the first-line test for IDs, as well as other targeted methylation analysis methods including pyrosequencing, methylation specific-PCR, bisulfite sequencing, and combined bisulfite restriction analysis. Furthermore, array-based methylation analysis and methylation analysis using short-read next-generation sequencing, such as whole genome bisulfite sequencing (WGBS) and reduced-representation bisulfite sequencing, are used for genome-wide methylation analysis. The conventional methylation analysis methods require additional processing, such as bisulfite treatment or methylation-sensitive restriction enzyme treatment, and assess the methylation levels of CpGs without distinguishing between paternal and maternal alleles. In targeted methylation analysis, only several CpGs within the DMRs are evaluated. In addition, to detect rare SNVs and SVs in patients with non-characteristic aberrant methylation in the DMRs, various methods, such as array-based comparative genomic hybridization analysis, Sanger sequencing, exome sequencing, amplicon sequencing, and whole genome sequencing, are required.

Nanopore-based long-read sequencing (LRS) (Oxford Nanopore Technologies, ONT) analyzes the electrical current intensity when the genomic DNA passes through a pore protein and obtains sequence reads 10–100 kb long together with single-molecule DNA modification, such as 5mC [9, 10]. Because of the disuse of bisulfite or methylation-sensitive restriction enzyme treatment, LRS represents a more accurate DNA methylation status than conventional methylation analysis. In addition, phasing analysis based on single-nucleotide polymorphism (SNPs) and indels on alleles shows the parental origin of each read [11] and clarifies the parental origin of structural abnormalities and methylation levels in the DMRs on each parental allele. However, because of low read depth in targeted regions, the whole-genome LRS is expensive for obtaining sufficient reads. Recently, adaptive sampling was developed for targeted sequencing. Targeted-LRS (T-LRS) using adaptive sampling enriches 0.1–10% of the whole genome region and obtains four to five times the read depth compared to whole-genome LRS [12, 13]. Genetic diagnosis of IDs using LRS has recently been reported in cases with Beckwith-Wiedemann syndrome, Silver-Russell syndrome (SRS),

Table 1 Summary of the eight major imprinting disorders and the multi-locus imprinting disturbance

Disease name	ID-responsible regions	ID-responsible DMRs	Genetic causes				Main clinical features	Ref
			Epi	UPD	SVs	SNVs		
TNDM	6q24	*PLAGL1*:alt-TSS	LOM	UPD(6)pat	dup(6q24)pat	*ZFP57*	SGA, TNDM, macroglossia, abdominal wall defects	2
SRS	11p15.5	*H19/IGF2*:IG	LOM	UPD(11)mat	*IGF2, CDKN1C, PLAG1, HMGA2*		SGA-SS, relative macrocephaly at birth, body asymmetry, prominent forehead, feeding difficulties	2
	Chr 7	*GRB10*:alt-TSS	GOM	UPD(7)mat	–			
		MEST:alt-TSS	GOM					
BWS	11p15.5	*H19/IGF2*:IG	GOM	UPD(11)pat	dup(11p15)pat, OBS, *KCNQ1*	*KCNQ1*, *CDKN1C*, OBS	Macroglossia, exomphalos, lateralized overgrowth, tumors, hyperinsulinism, placental mesenchymal dysplasia	2
		KCNQ1OT1:TSS	LOM					
TS14	14q32.2	*MEG3/DLK1*:IG	LOM	UPD(14)mat	del(14q32)pat	–	SGA-SS, neonatal hypotonia, feeding difficulties, precocious puberty, scoliosis, small feet and hands	2
		MEG3:TSS	LOM					
KOS	14q32.2	*MEG3/DLK1*:IG	GOM	UPD(14)pat	del(14q32)mat	–	Facial gestalt, abdominal wall defect, bell-shaped small thorax, coat-hanger ribs, intellectual disability	2
		MEG3:TSS	GOM					
PWS	15q11q13	*SNURF*:TSS	GOM	UPD(15)mat	del(15q11q13)pat	–	PNGR, intellectual disability, neonatal hypotonia, hyperphagia, hypogenitalia, obesity	2
AS	15q11q13	*SNURF*:TSS	LOM	UPD(15)pat	del(15q11q13)mat	*UBE3A*	Severe intellectual disability, microcephaly, no speech, unmotivated laughing, ataxia, seizures, scoliosis	2
PHP1B	20q13.32	*GNAS-NESP*:TSS	GOM	UPD(20)pat	dup(20q13)pat, del(20q13)mat, *STX16*	–	Resistance to parathyroid hormone, Albright hereditary osteodystrophy, obesity	2
		GNAS-AS1:TSS	LOM					
		GNAS-XL:Ex1	LOM					
		GNAS-AB:TSS	LOM					
	Chr6	–	–	UPD(6)mat	–	–	IUGR, ambiguous genitalia	4
	Chr7	–	–	UPD(7)pat	–	–	Overgrowth, developmental delay	5
	Chr16	–	–	UPD(16)mat	–	–	SGA-SS	6

Table 1 (continued)

Disease name	ID-responsible regions	ID-responsible DMRs	Genetic causes				Main clinical features	Ref
			Epi	UPD	SVs	SNVs		
	Chr20	–	–	UPD(20)mat	–	–	SGA-SS, feeding difficulties, hypersensitivity to hormones	2
MLID	Multiple	Multiple	LOM > GOM	–	–	*PADI6, KHDC3L, NLRP2/5/7, ZNF445, ZFP57*	Various phenotypes	7, 8

TNDM transient neonatal diabetes mellitus, *SRS* Silver-Russell syndrome, *BWS* Beckwith-Wiedemann syndrome, *TS14* Temple syndrome, *KOS* Kagami-Ogata syndrome, *PWS* Prader-Willi syndrome, *AS* Angelman syndrome, *PHP1B* pseudohypoparathyroidism type 1B, *MLID* multi-locus imprinting disturbance, *ID* imprinting disorder, *Chr* chromosome, *DMR* differentially methylated region, *TSS* transcription start site, *IG* intergenic, *Ex* exon, *Epi* epimutation; *LOM* loss of methylation, *GOM* gain of methylation, *UPD* uniparental disomy, *UPD(#)mat* maternal UPD of chromosome #, *UPD(#)pat* paternal UPD of chromosome #, *SV* structural variant, *dup(#)pat* corresponds to a duplication of the paternal allele at # region, *dup(#)mat* corresponds to a duplication of the maternal allele at # region, *del(#)pat* corresponds to a deletion of the paternal allele at # region, *del(#)mat* corresponds to a deletion of the maternal allele at # region, *SNV* single nucleotide variant, *OBS* OCT4/SOX2 binding site, *SGA* small for gestational age, *SGA-SS* SGA with short stature, *PNGR* postnatal growth restriction, *IUGR* intrauterine growth restriction

Kagami-Ogata syndrome (KOS), Temple syndrome (TS14), Angelman syndrome, Prader-Willi syndrome, and PHP1B, although these reports focused on genetic testing for each ID [14–19]. A T-LRS system targeting all imprinted regions and ID-responsible genes would be a more effective and informative diagnostic and research tool than conventional analyses combining the various analysis methods.

Here, we established a T-LRS system including 6101 CpGs on 78 DMRs and 22 genes and defined a normal range of methylation index in CpGs for each parental allele and the total. Moreover, we confirmed the usefulness of T-LRS in two patients with previously diagnosed MLID and nine cases with suspected IDs.

Methods

Nanopore sequencing and data analysis

Design of target regions

We included 78 reported DMRs [7, 20, 21], 8 ID-related genes, and 14 MLID causative genes in target regions (Table 2 and Additional file 1: Table S1). Based on previous reports, we classified 15 DMRs as clinically associated DMRs (CA-DMRs) functioning as imprinting control centers for imprinted genes related to IDs, 35 DMRs as non-clinical DMRs (NC-DMRs) with unknown function but differentially methylated, and 28 DMRs without consensus as to whether they are CA-DMRs or NC-DMRs as unannotated DMRs [7]. We defined the previously reported locus for the DMRs [7, 20, 21] plus over 100-kb margins on both sides as each target region of DMR. In the imprinted regions on chromosomes 6, 11, 14, 15, and 20, we set as the target region with 2–3 Mb including the DMRs and imprinted genes. The total sequencing region was 36,589,493 bp, equivalent to approximately 1.2% of the genome.

Subjects

First, we included six healthy controls, comprising three males and three females, and two patients with MLID for validation purposes. Patient 1 with MLID had a homozygous pathogenic variant in *ZNF445* and showed severe prenatal and postnatal growth failure [8]. Patient 2 with MLID presented with developmental delay and prenatal and postnatal growth failure, and the mother of Patient 2 had a heterozygous pathogenic variant in *NLRP2* [22]. MLID in both patients was identified by multi-locus methylation analysis for ID-responsible DMRs using MS-MLPA. Next to verify the usefulness of T-LRS in epigenetic diagnosis, we applied the T-LRS system to nine cases with suspected KOS, PHP1B, and SRS, based on characteristic clinical features for each disease [23–25].

Sample preparation

Genomic DNA from leukocytes was extracted by the Monarch HMW DNA Extraction Kit for Cells & Blood (New England Biolabs) or Gentra Puregene Blood Kit (Qiagen) according to the manufacturer's instructions. DNA samples (2–3 μg) were sheared to 10–15 kb using g-TUBE (Covaris). We removed small DNA fragments in the samples using the Short Read Eliminator Kit (Pacific Biosciences). According to the manufacturer's protocol, we prepared Nanopore sequencing libraries using the DNA Ligation Sequencing Kit V14 (ONT), loaded the libraries on MinION or PromethION flow cells (R10.4.1), and sequenced the libraries with the GridION Mk1 or PromethION 2 solo device under MinKNOW v22.12.5 or v23.11.7 (ONT) control. To obtain sufficient reads, we used two MinION flow cells in Controls 1–4 and one PromethION flow cell in Controls 5 and 6 and patients with MLID. We performed two wash and reload processes and then sequenced.

Table 2 List of target regions

CA-DMRs (n = 15)	*ZDBF2/GPR1*:IG-DMR	*IGF1R*:Int2-DMR	*ZBTB8B*	*IGF2*
PLAGL1:alt-TSS-DMR	*NAP1L5*:TSS-DMR	*ZNF597*:3′-DMR	*OSCP1*	*KCNQ1*
GRB10:alt-TSS-DMR	*VTRNA2-1*:DMR	*ZNF597*:TSS-DMR	*C1orf177*	*CDKN1C*
MEST:alt-TSS-DMR	*FAM50B*:TSS-DMR	*ZNF331*:alt-TSS-DMR1	*BRDT*	*UBE3A*
H19/IGF2:IG-DMR	*IGF2R*:Int2-DMR	*ZNF331*:alt-TSS-DMR2	*LOC101928118*	*GNAS (Gsα)*
IGF2:Ex9-DMR	*WDR27*:Int13-DMR	*MCTS2P*:TSS-DMR	*PYHIN1*	*STX16*
IGF2:alt-TSS-DMR	*PEG10*:TSS-DMR	*NNAT*:TSS-DMR	*OBSCN*	**MLID causative genes (n = 14)**
KCNQ1OT1:TSS-DMR	*SVOPL*:alt-TSS-DMR	*L3MBTL1*:alt-TSS-DMR	*GREM2_MIR1273E*	*PADI6*
MEG3/DLK1:IG-DMR	*HTR5A*:TSS-DMR	*WRB*:alt-TSS-DMR	*LOC151121*	*ZNF445*
MEG3:TSS-DMR	*ERLIN2*:Int6-DMR	*SNU13*:alt-TSS-DMR	*C2orf27B*	*WHSC1*
SNURF:TSS-DMR	*PEG13*:TSS-DMR	**Unannotated DMRs (n = 28)**	*DLX2_AS1*	*ZAR1*
PEG3:TSS-DMR	*FANCC*:Int1-DMR	*JAKMIP1*:Int2-DMR	*SMOC2*	*ZFP57*
GNAS-NESP:TSS-DMR	*INPP5F*:Int2-DMR	*RPS2P32*:TSS-DMR	*MAD1L1*	*KHDC3L*
GNAS-AS1:TSS-DMR	*RB1*:Int-DMR	*LOC101927815_2*	*LOC101927815_1*	*OOEP*
GNAS-XL:Ex1-DMR	*MEG8*:Int2-DMR	*CHD7*	*COL4A2*	*ATF7IP*
GNAS-A/B:TSS-DMR	*MKRN3*:TSS-DMR	*TRAPPC9_2*	*CDC16*	*TLE6*
NC-DMRs (n = 35)	*MAGEL2*:TSS-DMR	*PSCA*	*TIGD7*	*UHRF1*
PPIEL:Ex1-DMR	*NDN*:TSS-DMR	*PTCHD3:TSS-DMR*	*ANKRD20A11P*	*NLRP7*
DIRAS3:Ex2-DMR	*SNRPN*:alt-TSS-DMR	*LPAR6:TSS-DMR*	**ID-related genes (n = 8)**	*NLRP2*
DIRAS3:TSS-DMR	*SNRPN*:Int1-DMR1	*SORD*	*PLAG1*	*NLRP5*
GPR1:AS-TSS-DMR	*SNRPN*:Int1-DMR2	*MTRNR2L4*	*HMGA2*	*TRIM28*

CA clinically associated, *DMR* differentially methylated region, *TSS* transcription start site, *IG* intergenic, *Ex* exon, *Int* intron, *NC* non-clinical, *ID* imprinting disorder, *MLID* multi-locus imprinting disturbance

Base-calling and mapping

All data were base-called together with information on 5mC and cytosine (C) in each CpG using Guppy 6.4.6 (Controls 1–4) (dna_r10.4.1_e8.2_400bps_modbases_5mc_cg_hac.cfg, ONT) [26] or Dorado 7.2.13 (Controls 5 and 6, Patients 1 and 2, and Cases 1–9) (dna_r10.4.1_e8.2_400bps_5khz_modbases_5mc_cg_sup_prom.cfg, ONT) [27]. Reads were aligned to GRCh38 with decoy [28] using minimap2 [29]. PEPPER-Margin-DeepVariant (pepper_deepvariant_r0.8-gpu.sif) called SNV and indel variants, added to haplotype information based on the SNV and indel variants to each read, and formatted the analysis results as BAM files [11]. We visualized the BAM files on the Integrative Genomics Viewer (IGV) [30]. Coverage of target regions was calculated using Samtools depth (v1.13) [31]

Set normal ranges of methylation index of the DMRs for each parental allele

We calculated the methylation index (MI) (ranging from 0 to 1) of a single CpG by adding the MI of the neighboring sense and antisense strands in normal controls with Modkit [32], which produces the MI by dividing the number of reads having methylated CpGs by the total number of reads having unmethylated CpGs and methylated CpGs for each haplotype. We used the reads having 0.7 or more probability of 5mC (methylated) and 0.3 or less probability of 5mC (unmethylated cytosine, C) for the methylation analysis. After excluding CpGs with a read count under 10, we calculated the MI of each CpG on haplotype 1 and haplotype 2 and produced the total MI of the CpG by averaging MI on both haplotypes. Then we defined the normal range of the MI for each CpG as the minimum and maximum MI detected across Controls 1–6. We produced the median MI (MMI) of CpGs within each DMR. According to the methylation pattern of each DMR reported previously, haplotypes 1 and 2 were assigned to the maternal and paternal alleles, respectively. We calculated the difference in the MIs of CpGs within the DMRs between haplotypes 1 and 2 as ΔMI and produced the median of ΔMI (ΔMMI) of all CpGs in each DMR and an average of all controls' ΔMMI in all CpGs. The DMRs with ≥ 0.75 on average of all controls' ΔMMI were defined as "Complete-DMR", 0.25–0.75 as "Partial-DMR", and ≤ 0.25 as "Non-DMR". If a control had obviously different MMIs or ΔMMIs in the DMRs from those in other controls, we checked the reads in the control on IGV. When these reads were not properly classified into haplotypes 1 and 2, we processed these

MIs as missing values and classified the DMRs as a phasing error.

Validation of reproducibility for MIs at each CpG

To evaluate the reproducibility of MIs within the same sample, we conducted validation experiments in Controls 1, 2, and 3. In each experiment, we used a single PromethION flow cell (R10.4.1), performed base-calling with Guppy 6.4.6 (dna_r10.4.1_e8.2_400bps_modbases_5mc_cg_hac.cfg, ONT) [26], and calculated MIs for each CpG using Modkit [32]. We extracted CpGs with a read count exceeding 10 per haplotype in both the primary analysis and validation analysis and calculated the total MI for each CpG by averaging the MIs on both haplotypes. Subsequently, we examined the correlations of the MI for each CpG between the primary and validation experiments in Controls 1–3. The bivariate correlation of the MIs between the primary and validation experiments was assessed by Pearson's correlation coefficient.

Methylation analysis for patients with MLID

To compare the methylation levels of CpGs measured by array-based methylation analysis using the Infinium MethylationEPIC Kit (EPIC) (Illumina) and T-LRS, we conducted T-LRS with one PromethION flow cell on Patients 1 and 2 each. We selected CpGs examined by both EPIC and LRS, produced MIs, and evaluated the methylation status in the DMRs using both methods. In LRS, when both haplotypes 1 and 2 had fewer than 10 reads for a CpG, we used the combined read count of haplotypes 1 and 2 together with the unphased reads. We conducted array-based methylation analysis based on previous reports [8]. Background subtraction was applied, and CpGs with detection P values > 0.01 and/or no signal intensities were excluded, as well as those on the sex chromosomes. After excluding CpGs showing age-related drift and sex bias, we obtained β values indicating the MIs. In array-based methylation analysis using EPIC, we defined an aberrant DMR with |MMI| > 3 standard deviations (SDs) obtained from the mean of the MMI for a DMR in 16 controls, as previously reported [22, 33]. In LRS, we defined an aberrantly methylated DMR with |MMI| > 3 SDs obtained from the mean of MMI in six healthy controls.

(Epi)genetic analysis using LRS in cases with suspected IDs

To verify the usefulness of T-LRS in epigenetic diagnosis, we applied the T-LRS system to nine cases with suspected KOS, PHP1B, and SRS, exhibiting characteristic clinical features for each disease [23–25]. The clinical features are shown in Additional file 2: Table S2. We used a single PromethION flow cell (R10.4.1) in each case, base-called with Dorado 7.2.13 (dna_r10.4.1_e8.2_400bps_5khz_modbases_5mc_cg_sup_prom.cfg, ONT) [27], and calculated MIs with modkit [32]. When both haplotypes 1 and 2 had fewer than 10 reads for a CpG, we used the combined read count of haplotypes 1 and 2 together with the unphased reads. We extracted CpGs examined by both LRS and MS-MLPA Probe-mix ME034 in all cases (MRC-Holland). Subsequently, we used MS-MLPA Probe-mix ME034 in all cases and ME031 in a case with PHP1B, which detected a *STX16* deletion. Furthermore, we performed microsatellite marker analysis in some cases with methylation abnormalities and without structural abnormalities.

Results

Coverage in target regions

We conducted T-LRS in all controls and processed LRS sequence data into BAM files with methylation and phasing information. We obtained a mean coverage of 60 reads in Controls 1 to 4 using two MinION flow cells and 120 reads in Control 5 and 160 reads in Control 6 using a single PromethION flow cell (Additional file 1: Table S1). Initially, we could not obtain the aligned reads for the *H19*-DMR due to multiple hits. After excluding the chr11_KI270721v1_random from the reference fasta file (GRCh38 with decoy), we correctly obtained the reads aligned for the *H19*-DMR. The *ZFP57*, *NLRP2*, and *NLRP7* regions had lower coverage than the others. Visualized methylation and phase information for the *PLAGL1*:alt-transcription start site (TSS)-DMR in Control 1 on the IGV is shown in Fig. 1.

Normal range of MI in each CpG and characteristic of DMRs

We present the results of methylation analysis using T-LRS in each CpG within the DMRs for each haplotype in Controls 1–6 in Additional file 3: Table S3, A-F and summarized these data in Table 3. We obtained the MIs of CpGs within all DMRs using Modkit from the BAM file with methylation and phase information. We classified the *VTRNA2-1*:DMR in Control 2, the *HTR5A*:TSS-DMR in Control 5, the *GNAS-XL*:exon 1 (Ex1)-DMR in Control 3, and the *SNU13*:alt-TSS-DMR in Controls 1 and 6 as phasing errors (Additional file 3: Table S3, C). The median number of reads with 5mC and C in all DMRs in Controls 1, 2, 3, 4, 5, and 6 was 51 (min–max 0–91), 47 (0–85), 45 (0–69), 44 (0–83), 81 (0–152), and 81 (0–185), respectively. The percentage of the median number of reads with 5mC and C for total reads in all DMRs was 50–80% in controls. We classified the 78 DMRs into 33 Complete-DMRs, 25 Partial-DMRs, and 20 Non-DMRs according to the definitions given in the "Methods" section (Table 4). Of the CA-DMRs, all but the *IGF2*:Ex9-DMR, *IGF2*:alt-TSS-DMR, and *MEG3/DLK1*:IG-DMR were classified as Complete-DMRs. Of

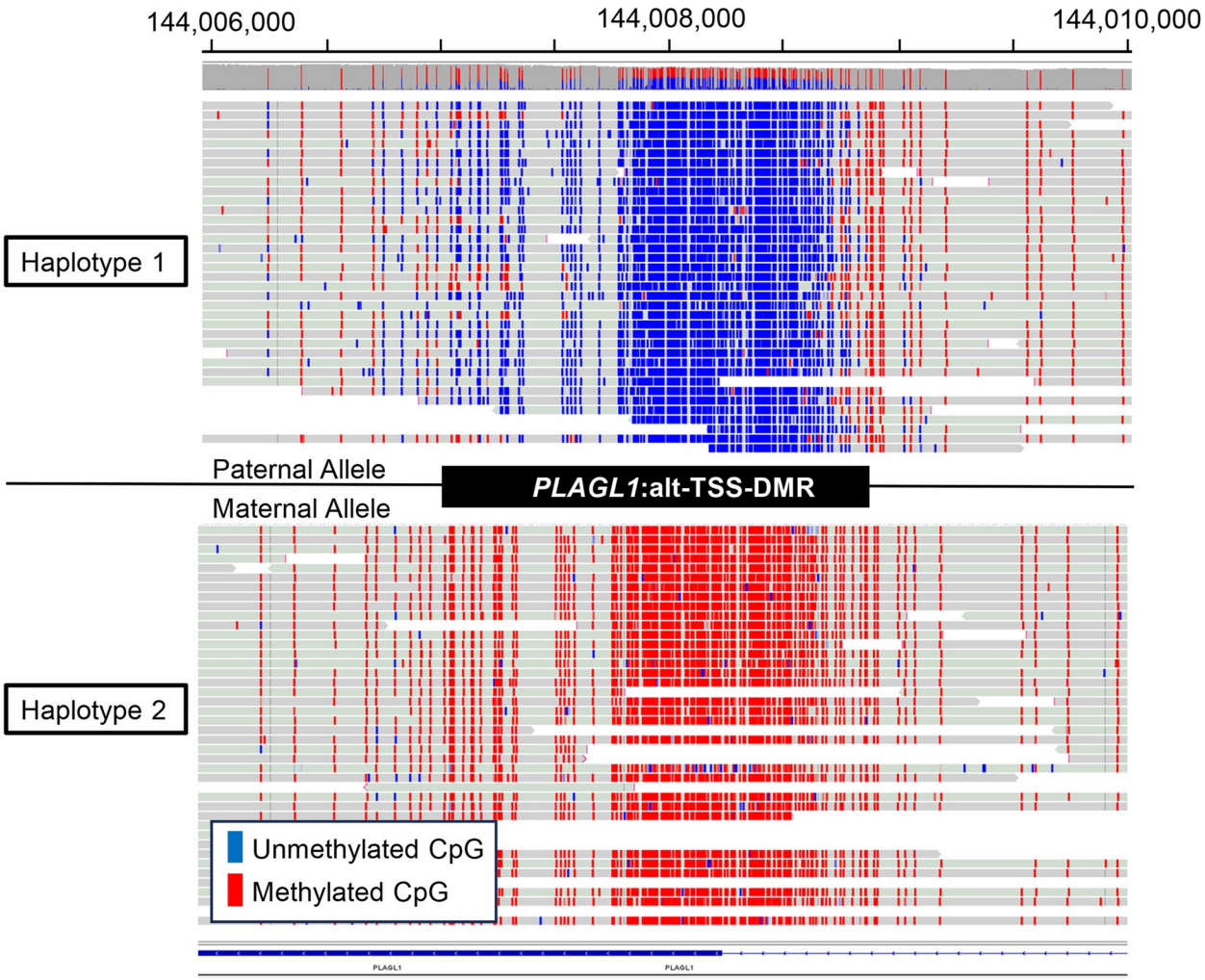

Fig. 1 The *PLAGL1*:alt-TSS-DMR on the Integrative Genomics Viewer. The reads classified into haplotype 1 are the paternally inherited allele and reads into haplotype 2 are the maternally inherited allele. The blue boxes indicate unmethylated CpGs with 0.3 or less probability of 5mC, the red boxes indicate methylated CpGs with 0.7 or more probability of 5mC, the gray reads indicate sense-strand reads, and the light green reads indicate antisense-strand reads. TSS, transcription; DMR, differentially methylated region

NC-DMRs, only the *MKRN3*:TSS-DMR was classified as a Non-DMR, but the first quarter of the region satisfied the definition of the partial-DMR (Additional file 1: Table S1 and Additional file 4: Fig. S1). Of the unannotated DMRs, no DMRs were classified as Complete-DMRs. Based on the previously reported methylation patterns of CA-DMRs [7], we determined the parental origin of each haplotype and showed the normal range of the MIs in all CpGs within 15 CA-DMRs (Fig. 2). The patterns of normal range of MIs of CpGs in the CA-DMR were various. The beginning and end of the DMR tended to hypermethylation. The *PLAGL1*:alt-TSS-DMR, *IGF2*:Ex9-DMR, *IGF2*:alt-TSS-DMR, *MEG3/DLK1*:IG-DMR, and *GNAS-AS1*:TSS-DMR showed wide normal MI ranges in paternal, maternal, and the total due to differences in MIs among controls. On the other hand, the *GRB10*:alt-TSS-DMR, *MEST*:TSS-DMR, *H19*-DMR, *KCNQ1OT1:*TSS-DMR, *MEG3*:TSS-DMR, *SNURF*:TSS-DMR, *PEG3*:TSS-DMR, *GNAS-NESP*:TSS-DMR, *GNAS-XL*:Ex1-DMR, and *GNAS-A/B*:TSS-DMR had narrow normal MI ranges in paternal, maternal, and the total. We compared the position and the numbers of CpGs evaluated by different methylation analyses, such as EPIC, MS-MLPA Probe-mix ME034 (MRC-Holland), pyrosequencing, and LRS (Fig. 2 and Table 5). Most CpGs evaluated by MS-MLPA and pyrosequencing in our previous study [22, 34] were located on the regions with markedly different MIs between the maternal and paternal alleles (Fig. 2 and Additional file 5: Table S4). However, as shown in Additional file 5: Table S4, some CpGs in

Table 3 Summary of methylation information for DMRs in controls

DMR	Imprint origin	Chr	CpG	Read counts on paternal allele	Read counts on maternal allele	MMI of paternal allele	MMI of maternal allele	Total MMI			ΔMMI (pat–mat)
				Median (min–max)	Median (min–max)	Median (min–max)	Median (min–max)	Mean	3 SD	−3 SD	All (mean)
PPIEL:Ex1	Oocyte	1	38	24 (0–70)	26 (0–72)	0.41 (0.31–0.56)	0.99 (0.91–1.00)	0.69	0.86	0.51	0.56
DIRAS3:TSS	Oocyte	1	39	31 (0–50)	29.5 (0–49)	0.47 (0.24–0.57)	0.95 (0.76–0.97)	0.68	0.82	0.54	0.48
DIRAS3:Ex2	Oocyte	1	83	22 (0–51)	18.5 (0–43)	0.08 (0.05–0.13)	0.95 (0.91–0.98)	0.51	0.54	0.49	0.86
ZDBF2/GPR1:IG	Sper-Sec	2	438	28 (20–69)	24 (18–57)	0.97 (0.94–1.00)	0.34 (0.15–0.52)	0.65	0.82	0.48	0.64
JAKMIP1:Int2	Oocyte	4	82	16.5 (0–72)	20 (0–60)	0.94 (0.87–0.97)	0.42 (0.40–0.60)	0.69	0.84	0.54	0.48
NAP1L5:TSS	Oocyte	4	57	28 (15–69)	34 (26–80)	0.00	1.00	0.50	0.50	0.50	1.00
VTRNA2-1	Oocyte	5	78	19 (0–27)	25 (0–31)	0.02 (0.00–0.09)	0.94 (0.77–0.96)	0.48	0.57	0.39	0.87
FAM50B:TSS	Oocyte	6	89	31 (23–58)	37 (22–82)	0.04 (0.00–0.10)	0.99 (0.97–1.00)	0.52	0.56	0.47	0.95
PLAGL1:alt-TSS	Oocyte	6	142	35.5 (24–58)	32 (27–60)	0.00 (0.00–0.38)	1.00 (0.81–1.00)	0.52	0.63	0.42	0.88
IGF2R:Int2	Oocyte	6	74	28 (25–54)	30.5 (20–59)	0.23 (0.16–0.56)	1.00 (0.66–1.00)	0.60	0.66	0.54	0.63
WDR27:Int13	Oocyte	6	57	27 (18–51)	31.5 (16–58)	0.03 (0.00–0.04)	0.96 (0.90–1.00)	0.49	0.55	0.44	0.93
RPS2P32:TSS	Oocyte	7	55	27 (0–46)	28.5 (0–46)	0.72 (0.52–1.00)	0.00 (0.00–0.53)	0.46	0.80	0.12	0.67
GRB10:alt-TSS	Oocyte	7	170	24 (4–61)	35 (12–64)	0.04 (0.02–0.05)	0.98 (0.96–1.00)	0.51	0.53	0.48	0.94
PEG10:TSS	Oocyte	7	119	27 (13–88)	31 (9–64)	0.00 (0.00–0.13)	0.98 (0.94–1.00)	0.51	0.59	0.42	0.95
MEST:alt-TSS	Oocyte	7	225	21 (9–57)	33.5 (9–80)	0.00 (0.00–0.07)	0.99 (0.96–1.00)	0.50	0.53	0.47	0.97
SVOPL:alt-TSS	Oocyte	7	32	32 (21–57)	33.5 (19–67)	0.04 (0.00–0.10)	0.88 (0.78–0.96)	0.45	0.56	0.34	0.82
HTR5A:TSS	Oocyte	7	55	22 (14–62)	33 (27–82)	0.33 (0.25–0.40)	0.92 (0.86–0.94)	0.63	0.73	0.54	0.58
LOC101927815_2	Oocyte?	8	12	21.5 (16–31)	17 (15–28)	0.49 (0.18–0.82)	0.00 (0.00–0.07)	0.28	0.66	−0.11	0.50
ERLIN2:Int6	Oocyte	8	37	20 (0–42)	22 (0–41)	0.06 (0.00–0.14)	0.90 (0.76–0.93)	0.48	0.64	0.32	0.81
CHD7	Oocyte?	8	27	34 (23–71)	32 (24–59)	0.95 (0.85–1.00)	0.19 (0.12–0.43)	0.58	0.80	0.36	0.72
PEG13:TSS	Oocyte	8	192	20 (17–32)	25.5 (18–30)	0.00 (0.00–0.08)	1.00 (0.96–1.00)	0.51	0.56	0.46	0.97
TRAPPC9_2	Oocyte?	8	16	22.5 (0–30)	21.5 (0–36)	0.76 (0.64–0.97)	0.57 (0.20–0.75)	0.65	1.15	0.15	0.26
PSCA	Oocyte?	8	2	28 (17–39)	27.5 (15–42)	0.56 (0.01–0.97)	0.01 (0.00–0.44)	0.29	0.94	−0.37	0.42
FANCC:Int1	Oocyte	9	28	20 (17–32)	25.5 (18–30)	0.13 (0.04–0.22)	0.95 (0.76–1.00)	0.52	0.65	0.39	0.78
PTCHD3:TSS	Oocyte	10	58	14.5 (0–43)	15.5 (0–43)	1.00 (0.92–1.00)	0.37 (0.21–0.44)	0.66	0.77	0.58	0.62
INPP5F:Int2	Oocyte	10	51	28 (20–63)	34 (15–71)	0.41 (0.36–0.48)	1.00 (0.97–1.00)	0.70	0.77	0.63	0.58
H19/IGF2:IG	Sperm	11	249	16 (4–26)	11.5 (8–38)	1.00 (0.97–1.00)	0.00 (0.00–0.03)	0.50	0.50	0.50	0.99
IGF2:Ex9	Second	11	63	28.5 (14–46)	25 (12–38)	0.93 (0.86–0.94)	0.39 (0.24–0.58)	0.64	0.81	0.48	0.53
IGF2:alt-TSS	Sperm	11	38	18 (14–51)	20.5 (16–36)	0.89 (0.73–0.90)	0.14 (0.09–0.20)	0.50	0.59	0.40	0.72
KCNQ1OT1:TSS	Oocyte	11	190	24.5 (6–36)	25 (8–44)	0.00 (0.00–0.05)	0.94 (0.92–1.00)	0.49	0.52	0.46	0.94
RB1:Int	Oocyte	13	195	22.5 (7–60)	25 (5–44)	0.22 (0.06–0.39)	0.97 (0.71–1.00)	0.70	1.33	0.06	0.72
LPAR6:TSS	Oocyte	13	25	8 (0–31)	7.5 (0–28)	0.73 (0.59–0.88)	0.35 (0.20–0.63)	0.56	0.89	0.24	0.26
MEG3/DLK1:IG	Sperm	14	62	30 (18–54)	30.5 (20–58)	0.98 (0.95–1.00)	0.47 (0.44–0.58)	0.73	0.79	0.67	0.49
MEG3:TSS	Second	14	188	28.5 (20–53)	24 (18–61)	0.97 (0.96–1.00)	0.04 (0.00–0.07)	0.51	0.54	0.47	0.94
MEG8:Int2	Second	14	43	23.5 (10–36)	26 (11–47)	0.00 (0.00–0.09)	0.97 (0.88–0.98)	0.50	0.57	0.42	0.93

Table 3 (continued)

DMR	Imprint origin	Chr	CpG	Read counts on paternal allele	Read counts on maternal allele	MMI of paternal allele	MMI of maternal allele	Total MMI			ΔMMI (pat–mat)
				Median (min–max)	Median (min–max)	Median (min–max)	Median (min–max)	Mean	3 SD	−3 SD	All (mean)
MAGEL2:TSS	Second	15	51	18 (12–48)	24.5 (10–46)	0.26 (0.00–0.61)	0.79 (0.60–0.96)	0.51	0.58	0.45	0.51
NDN:TSS	Second	15	108	24 (13–62)	24 (13–68)	0.09 (0.00–0.17)	0.82 (0.80–0.88)	0.48	0.57	0.40	0.75
SNRPN:alt-TSS	Second	15	19	26 (7–52)	24.5 (12–62)	0.13 (0.10–0.18)	0.94 (0.92–1.00)	0.55	0.58	0.51	0.81
SNRPN:Int1_1	Oocyte	15	44	27.5 (6–32)	21.5 (2–25)	0.07 (0.00–0.13)	0.81 (0.75–0.85)	0.46	0.54	0.37	0.74
SNRPN:Int1_2	Oocyte	15	45	29.5 (26–64)	22.5 (16–57)	0.10 (0.07–0.36)	0.75 (0.47–0.81)	0.43	0.53	0.33	0.57
SNURF:TSS	Oocyte	15	111	29 (1–74)	28.5 (2–87)	0.00 (0.00–0.07)	0.98 (0.96–1.00)	0.50	0.54	0.46	0.97
SORD	Oocyte?	15	12	13 (0–28)	12.5 (0–28)	0.52 (0.38–0.61)	0.12 (0.00–0.17)	0.30	0.43	0.17	0.41
IGF1R:Int2	Oocyte	15	54	22.5 (0–40)	23.5 (0–39)	0.11 (0.02–0.22)	0.91 (0.86–0.95)	0.51	0.58	0.44	0.79
MTRNR2L4	Sperm?	16	25	25 (0–35)	17.5 (0–25)	0.00 (0.00–0.05)	0.27 (0.17–0.48)	0.17	0.31	0.03	0.28
ZNF597:3′	Oocyte	16	29	23.5 (14–29)	23 (16–39)	0.18 (0.00–0.31)	1.00	0.58	0.76	0.40	0.83
ZNF597:TSS	Second	16	75	23.5 (0–31)	23 (0–29)	0.94 (0.90–1.00)	0.00	0.48	0.53	0.43	0.78
ZNF331:alt-TSS1	Oocyte	19	125	29 (17–62)	29 (24–67)	0.00 (0.00–0.04)	0.99 (0.94–1.00)	0.50	0.54	0.46	0.98
ZNF331:alt-TSS2	Oocyte	19	101	25.5 (13–60)	26.5 (8–48)	0.00	1.00 (0.98–1.00)	0.50	0.50	0.50	1.00
PEG3:TSS	Oocyte	19	220	26.5 (0–51)	25.5 (0–52)	0.04 (0.00–0.07)	0.99 (0.93–1.00)	0.51	0.52	0.48	0.94
MCTS2P:TSS	Oocyte	20	47	30.5 (7–58)	30 (17–53)	0.03 (0.00–0.32)	1.00 (0.77–1.00)	0.52	0.60	0.44	0.81
NNAT:TSS	Oocyte	20	135	22.5 (13–32)	27 (19–43)	0.30 (0.06–0.45)	1.00 (0.94–1.00)	0.62	0.83	0.41	0.72
L3MBTL1:alt-TSS	Oocyte	20	84	29.5 (13–71)	31 (21–65)	0.00 (0.00–0.03)	1.00 (0.91–1.00)	0.50	0.54	0.45	0.98
GNAS-NESP:TSS	Second	20	257	20 (4–67)	25 (2–56)	1.00 (0.99–1.00)	0.05 (0.04–0.08)	0.52	0.55	0.50	0.95
GNAS-AS1:TSS	Oocyte	20	128	15 (4–28)	16 (2–32)	0.00 (0.00–0.17)	0.93 (0.77–0.99)	0.49	0.61	0.37	0.86
GNAS-XL:Ex1	Oocyte	20	200	15 (4–19)	13 (3–22)	0.00 (0.00–0.05)	1.00 (0.96–1.00)	0.49	0.52	0.46	0.96
GNAS-A/B:TSS	Second	20	198	26.5 (11–65)	26 (13–55)	0.00	1.00 (0.96–1.00)	0.50	0.52	0.48	0.99
WRB:alt-TSS	Oocyte	21	42	11 (0–45)	15 (1–50)	0.19 (0.04–0.50)	1.00 (0.98–1.00)	0.60	0.90	0.30	0.76
SNU13:alt-TSS	Oocyte	22	62	18 (11–26)	19 (9–31)	0.00 (0.00–0.05)	0.98 (0.90–1.00)	0.49	0.56	0.42	0.95

DMR differentially methylated region, *Ex* exon, *TSS* transcription start site, *IG* intergenic, *Int* intron, *Sper-Sec* sperm DMR-secondary DMR, Second, secondary DMR, *Chr* chromosome, *MMI* median methylation index, *SD* standard deviation

Table 4 Characteristics of each DMR

Complete-DMRs (n = 33)	Partial-DMRs (n = 25)	Non-DMRs (n = 20)
DIRAS3:Ex2-DMR	*PPIEL*:Ex1-DMR	*ZBTB8B*
NAP1L5:TSS-DMR	*DIRAS3*:TSS-DMR	*OSCP1*
VTRNA2-1:DMR	*JAKMIP1*:Int2-DMR	*C1orf177*
FAM50B:TSS-DMR	*ZDBF2/GPR1*:IG-DMR	*BRDT*
PLAGL1:alt-TSS-DMR	*IGF2R*:Int2-DMR	*LOC101928118*
WDR27:Int13-DMR	*RPS2P32*:TSS-DMR	*PYHIN1*
GRB10:alt-TSS-DMR	*HTR5A*:TSS-DMR	*OBSCN*
PEG10:TSS-DMR	*LOC101927815_2*	*GREM2_MIR1273E*
MEST:alt-TSS-DMR	*CHD7*	*LOC151121*
SVOPL:alt-TSS-DMR	*TRAPPC9_2*	*C2orf27B*
ERLIN2:Int6-DMR	*PSCA*	*DLX2_AS1*
PEG13:TSS-DMR	*PTCHD3*:TSS-DMR	*GPR1-AS:TSS-DMR*
FANCC:Int1-DMR	*INPP5F*:Int2-DMR	*SMOC2*
H19/IGF2:IG-DMR	*IGF2*:Ex9-DMR	*MAD1L1*
KCNQ1OT1:TSS-DMR	*IGF2*:alt-TSS DMR	*LOC101927815_1*
MEG3:TSS-DMR	*RB1*:Int-DMR	*COL4A2*
MEG8:Int2-DMR	*LPAR6*:TSS-DMR	*CDC16*
SNRPN:alt-TSS-DMR	*MEG3/DLK1:IG-DMR*	*MKRN3:TSS-DMR*
SNURF:TSS-DMR	*MAGEL2*:TSS-DMR	*TIGD7*
IGF1R:Int2-DMR	*NDN*:TSS-DMR	*ANKRD20A11P*
ZNF597:3′:DMR	*SNRPN*:Int1-DMR1	
ZNF597:TSS-DMR	*SNRPN*:Int1-DMR2	
ZNF331:alt-TSS-DMR1	*SORD*	
ZNF331:alt-TSS-DMR2	*MTRNR2L4*	
PEG3:TSS-DMR	*NNAT:TSS-DMR*	
MCTS2P:TSS-DMR		
L3MBTL1:alt-TSS:DMR		
GNAS-NESP:TSS-DMR		
GNAS-AS1:TSS-DMR		
GNAS-XL:Ex1-DMR		
GNAS-A/B:TSS:DMR		
WRB:alt-TSS-DMR		
SNU13:alt-TSS-DMR		

DMR differentially methylated region, *Ex* exon, *TSS* transcription start site, *Int* intron, *IG* intergenic

the DMRs analyzed by EPIC were present in the regions without markedly different MIs between the paternal and maternal alleles (e.g., *MEST*:alt-TSS-DMR). In the comparison between primary and validation analyses, MIs at each CpG showed a high correlation in all three controls (Fig. 3 and Additional file 6: Table S5).

Comparison of the methylation patterns in the DMRs between LRS and array-based methylation analysis

We evaluated this T-LRS system in two patients with MLID having pathogenic variants of causative genes for MLID and compared MMI in the DMRs between T-LRS and array-based analysis using EPIC. We obtained sufficient sequence reads for DMRs (Additional file 7: Table S6), acquired 132.9 mean coverage for *ZNF445* in Patient 1 and 11.5 for *NLRP2* in Patient 2, and detected pathogenic variants in both patients (Additional file 4: Fig. S2). The methylation defect patterns of two patients with MLID in T-LRS were similar to those identified in array-based analysis, although T-LRS showed more aberrant methylated DMRs than array-based analysis (Fig. 4). In Patient 1, T-LRS identified the hypomethylated *H19*-DMR and *MEG3*:TSS-DMR and hypermethylated *MEG8*: intron 2 (Int2)-DMR, which were identical DMRs with the same methylation pattern detected by array-based methylation analysis. The hypomethylation of the *PPIEL*:Ex1-DMR, *DIRAS3*:TSS-DMR, *GPR1:AS*-TSS-DMR, *SVOPL*:alt-TSS-DMR, *HTR5A*:TSS-DMR, *IGF2*:Ex2-DMR, *IGF2*:alt-TSS-DMR, *ZNF597*:TSS-DMR, and *GNAS-A/B*:TSS-DMR and hypermethylation of the *GNAS-NESP*:TSS-DMR were identified only by T-LRS. In Patient 2, the hypomethylation of the *PPIEL*:Ex1-DMR, *DIRAS3*:Ex2-DMR, *DIRAS3*:TSS-DMR, *NAP1L5*:TSS-DMR, *GRB10*:alt-TSS-DMR, *PEG10*:TSS-DMR, *FANCC*:Int1-DMR, *INPP5F*:Int2-DMR, *H19*-DMR, *IGF2*:Ex2-DMR, *IGF2*:alt-TSS-DMR, *KCNQ1OT1*:TSS-DMR, *IGF1R*:Int2-DMR, *ZNF331*:alt-TSS-DMR1, *ZNF331*:alt-TSS-DMR2, *L3MBTL1*:alt-DMR, and *SNU13*:alt-TSS-DMR and hypermethylation of the *ZDB2/GPR1*:IG-DMR, *ZNF597*:TSS-DMR, and *MCTS2P*:TSS-DMR had an identical methylation pattern between T-LRS and array-based methylation analysis. The hypomethylation of the *FAM50B:*TSS-DMR, *NDN*:TSS-DMR, and *SNURF*:TSS-DMR and hypermethylation of the *WDR27*:Int2-DMR and *MEST*:alt-TSS-DMR were identified only by T-LRS. The *IGF2R*:Int2-DMR showed hypomethylation in LRS, but hypermethylation in array-based methylation analysis. The *NAP1L5*:TSS-DMR, which is a germline DMR methylated in oocytes, exhibited completely unmethylated and methylated haplotypes. Because the MMI in T-LRS was 0.5 in all controls, the SD of MMI in this DMR was 0, and we could not set the normal range. Overall, we obtained nearly equal analysis results in T-LRS compared to those using conventional analysis methods.

(Epi)genetic diagnosis using LRS in cases with suspected IDs

Case 1 had a clinical diagnosis of KOS and showed hypermethylation of the *MEG3*:TSS-DMR, hypomethylation of the *MEG8*:Int2-DMR, and loss of heterozygosity involving the region in LRS, suggesting isodisomy (Additional file 4: Fig. S3, A and B, and Additional file 8: Table S7, A and B). The same methylation defect pattern was identified by MS-MLPA analysis using Probe-mix ME034 (Additional file 4: Fig. S3C). Microsatellite marker

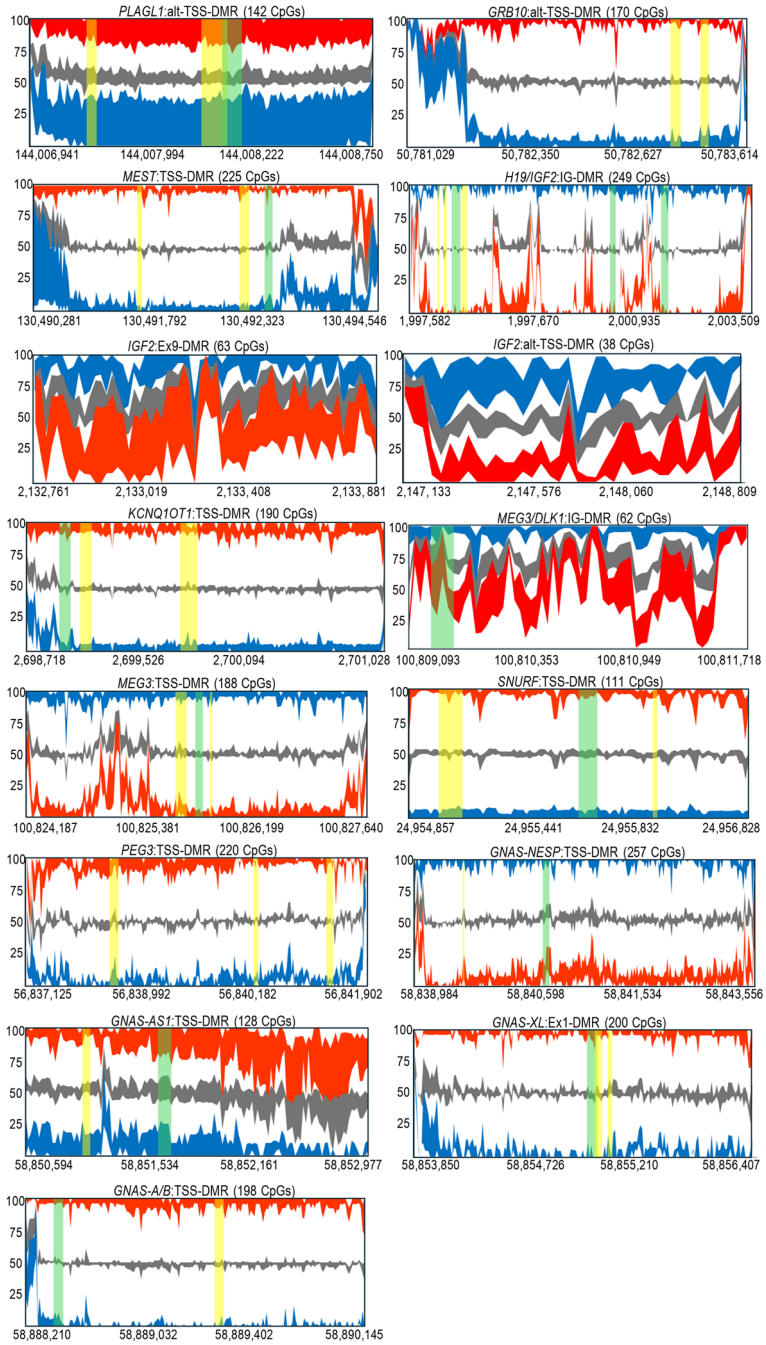

Fig. 2 The normal range of MIs in clinically associated-DMRs. The red area indicates the normal ranges of MIs on the maternal allele (minimum–maximum in six controls). The blue area indicates the normal ranges of MIs on the paternal allele (minimum–maximum in six controls). The gray area indicates the normal ranges of MIs in the total (minimum–maximum in six controls). The color-coded background indicates the locus of CpGs examined by methylation-specific multiple ligation-dependent probe amplification analysis (yellow) and pyrosequencing (green). MI, methylation index; DMR, differential methylated region; TSS, transcription start site; Ex, exon; IG, intergenic

analysis in Case 1 showed paternal isodisomy of chromosome 14 (Additional file 4: Fig. S3D). Case 2 had a clinical diagnosis of PHP1B and showed hypomethylation of the *GNAS:A/B*-DMR and a heterozygous microdeletion involving *STX16* (Additional file 4: Fig. S4, A-C and Additional file 8: Table S7, A and C). The same methylation defect pattern and deletion involving *STX16* were identified by MS-MLPA analysis using Probe-mix ME034 and

Table 5 Comparison of the number of CpG sites in the fifteen CA-DMRs evaluated by different methylation analyses

DMR	Number of CpGs			
	LRS	EPIC	MS-MLPA (ME034)	Pyrosequencing
PLAGL1:alt-TSS-DMR	142	14	14	9
GRB10:alt-TSS-DMR	170	9	11	0
MEST:alt-TSS-DMR	225	48	11	6
H19/IGF2:IG-DMR	249	34	10	18
IGF2:Ex9-DMR	63	10	0	0
IGF2:alt-TSS DMR	38	2	0	0
KCNQ1OT1:TSS-DMR	190	25	16	6
MEG3/DLK1:IG-DMR	62	0	0	5
MEG3:TSS-DMR	188	35	9	5
SNURF:TSS-DMR	111	10	9	5
PEG3:TSS-DMR	220	34	12	0
GNAS-NESP:TSS-DMR	257	23	2	6
GNAS-AS1:TSS-DMR	128	56	3	6
GNAS-XL:Ex1-DMR	200	7	10	7
GNAS-A/B:TSS-DMR	198	39	6	7

CA clinically associated, *DMR* differentially methylated region, *TSS* transcription start site, *IG* intergenic, *Ex* exon, *LRS* long-read sequencing, *EPIC* array-based methylation analysis using EPIC (Illumina), *MS-MLPA* methylation-specific multiple ligation-dependent probe amplification, *ME034* MS-MLPA Probe-mix ME034 (MRC-Holland)

ME031 (Additional file 4: Fig. S4, D and E). Case 3 also had a clinical diagnosis of PHP1B and showed hypomethylation of the *GNAS:A/B*-TSS-DMR, *GNAS-AS1*:TSS-DMR, and *GNAS-XL*:Ex1-DMR and hypermethylation of the *GNAS-NESP*:TSS-DMR (Additional file 4: Fig. S5, A and B, and Additional file 8: Table S7, A and D). The same methylation defect pattern was identified by MS-MLPA analysis using Probe-mix ME034 (Additional file 4: Fig. S5C). Due to the absence of parental samples, the etiology of Case 3 was unclear as to whether it was UPD or epimutation. Cases 4–8 had a clinical diagnosis of SRS and showed hypomethylation of the *H19/IGF2*:IG-DMR (Additional file 4: Fig. S6-10, A and B and Additional file 8: Table S7, A and E-I). The same methylation defect pattern was identified by MS-MLPA analysis using Probe-mix Me034 (Additional file 4: Fig. S6-10C). Case 9 also had a clinical diagnosis of SRS and showed hypomethylation of the *MEG3*:TSS-DMR and hypermethylation of the *MEG8*:Int2-DMR (Additional file 4: Fig. S11, A and B and Additional file 8: Table S7, A and J); therefore, Case 9 had a genetic diagnosis of TS14. The same methylation defect pattern was observed by MS-MLPA analysis using Probe-mix ME034 (Additional file 4: Fig. S11C). Microsatellite analysis for chromosome 14 in Case 9 revealed a biparental origin; therefore, the etiology in Case 9 was epimutation (Additional file 4: Fig. S11D). Overall, MIs in CpGs in which haplotype phasing was unavailable tended to deviate from the normal range (minimum and maximum of six controls) compared to those in which haplotype phasing was available.

Discussion

We established a comprehensive T-LRS system covering all DMRs and the regions associated with IDs and obtained sequence and methylation data simultaneously. Our T-LRS system revealed continuous methylation levels of CpGs on each parental allele in all ID-related DMRs. In comparison with a previous report that used nanopore LRS to analyze DNA methylation in the imprinted regions [35], there were slight variations in MIs due to differences in reagents (our Kit V14 vs. previous report Kit V9), flow cells (R10 vs. R9), methods (target vs. genome-wide) and subjects (6 controls vs. 6 patients), but the overall MI patterns appeared to be similar.

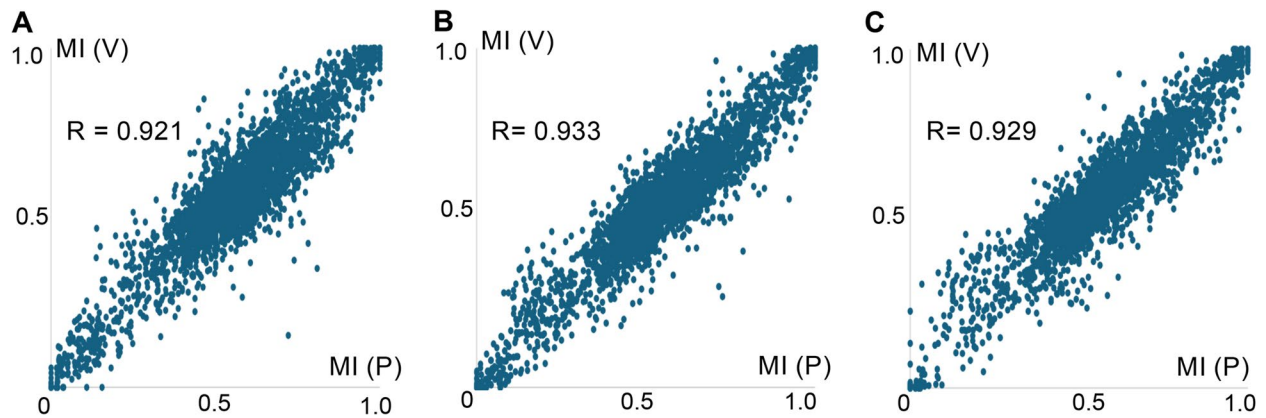

Fig. 3 Correlation of methylation indexes between primary and validation analyses. **A** Control 1. **B** Control 2. **C** Control 3. MI, methylation index; V, validation analysis; P, primary analysis

DMR	Long read sequencing				Methylation array			
	+ 3SD	–3SD	Pt. 1	Pt. 2	+ 3SD	–3SD	Pt. 1	Pt. 2
PPIEL :Ex1	0.72	0.62	0.62	0.21	0.78	0.59	0.68	0.47
DIRAS3 :Ex2	0.70	0.52	0.53	0.13	0.57	0.43	0.49	0.21
DIRAS3 :TSS	0.55	0.47	0.37	0.03	0.61	0.49	0.52	0.21
GPR1 :AS-TSS	1.05	0.92	0.49	0.95	0.98	0.93	0.95	0.95
ZDBF2/GPR1 :IG	0.55	0.50	0.51	0.81	0.70	0.55	0.66	0.93
NAP1L5 :TSS	0.50	0.50	0.47	0.00	0.64	0.57	0.60	0.19
VTRNA2-1	0.95	-0.17	0.39	0.06	0.95	–0.11	0.43	0.24
FAM50B :TSS	0.53	0.46	0.49	0.46	0.62	0.50	0.55	0.61
PLAGL1 :alt-TSS	0.67	0.39	0.50	0.50	0.61	0.51	0.55	0.58
IGF2R :Int2	0.66	0.54	0.57	0.50	0.65	0.44	0.54	0.72
WDR27 :Int13	0.52	0.50	0.50	0.55	0.81	0.37	0.59	0.66
GRB10 :alt-TSS	0.55	0.49	0.50	0.08	0.65	0.50	0.57	0.13
PEG10 :TSS	0.59	0.42	0.49	0.03	0.62	0.52	0.57	0.22
MEST :alt-TSS	0.54	0.46	0.50	0.59	0.68	0.54	0.58	0.67
SVOPL :alt-TSS	0.63	0.30	0.25	0.40	0.63	0.32	0.42	0.51
HTR5A :TSS	0.77	0.58	0.57	0.66	0.70	0.54	0.60	0.64
ERLIN2 :Int6	0.55	0.38	0.42	0.45	0.68	0.41	0.50	0.59
PEG13 :TSS	0.53	0.47	0.50	0.50	0.75	0.62	0.68	0.72
FANCC :Int1	0.63	0.40	0.53	0.00	0.59	0.33	0.42	0.23
INPP5F :Int2	0.81	0.60	0.76	0.45	0.78	0.67	0.73	0.65
H19/IGF2 :IG	0.53	0.49	0.00	0.03	0.68	0.55	0.52	0.24
IGF2 :Ex9	0.75	0.49	0.43	0.22	0.67	0.47	0.52	0.42
IGF2 :alt-TSS	0.44	0.36	0.22	0.06	0.57	0.42	0.44	0.24
KCNQ1OT1 :TSS	0.52	0.45	0.51	0.02	0.60	0.49	0.51	0.30
RB1 :Int2	0.65	0.47	0.48	0.55	0.68	0.52	0.58	0.59
MEG3 :TSS	0.54	0.48	0.04	0.50	0.67	0.57	0.41	0.63
MEG8 :Int2	0.58	0.44	0.97	0.55	0.75	0.64	0.79	0.70
MKRN3 :TSS	1.01	0.90	0.97	0.93	0.95	0.83	0.88	0.90
MAGEL2 :TSS	0.55	0.40	0.48	0.41	0.61	0.40	0.47	0.45
NDN :TSS	0.59	0.36	0.44	0.34	0.58	0.39	0.49	0.48
SNURF :TSS	0.53	0.47	0.49	0.46	0.64	0.54	0.59	0.58
SNRPN :alt-TSS	0.61	0.48	0.50	0.58	0.68	0.54	0.61	0.59
SNRPN :Int1-1	0.60	0.23	0.36	0.25	0.56	0.33	0.44	0.45
SNRPN :Int1-2	0.60	0.28	0.50	0.47	0.73	0.38	0.53	0.47
IGF1R :Int2	0.56	0.43	0.50	0.04	0.70	0.50	0.56	0.40
ZNF597 :3'	0.81	0.42	0.67	0.60	0.78	0.59	0.65	0.57
ZNF597 :TSS	0.54	0.41	0.39	0.93	0.64	0.45	0.56	0.78
ZNF331 :alt-TSS1	0.53	0.46	0.50	0.03	0.57	0.40	0.46	0.21
ZNF331 :alt-TSS2	0.50	0.49	0.50	0.00	0.62	0.48	0.53	0.12
PEG3 :TSS	0.53	0.48	0.50	0.50	0.67	0.55	0.61	0.61
MCTS2P :TSS	0.61	0.43	0.51	0.62	0.58	0.48	0.53	0.58
NNAT :TSS	0.95	0.49	0.64	0.69	0.79	0.64	0.68	0.71
L3MBTL1 :alt	0.53	0.46	0.49	0.17	0.66	0.49	0.57	0.43
GNAS-NESP :TSS	0.56	0.48	0.57	0.53	0.67	0.54	0.62	0.63
GNAS-AS1 :TSS	0.63	0.36	0.42	0.50	0.57	0.48	0.49	0.55
GNAS-XL :Ex1	0.57	0.45	0.50	0.50	0.60	0.48	0.53	0.57
GNAS-A/B :TSS	0.52	0.48	0.47	0.48	0.60	0.49	0.53	0.58
WRB :alt-TSS	0.87	0.08	0.53	0.22	0.58	0.44	0.49	0.33
SNU13 :alt-TSS	0.69	0.29	0.48	0.00	0.57	0.37	0.43	0.20

◀ **Fig. 4** Comparison of methylation index in the DMRs between methylation analyses. The values in the box show the median methylation index of the DMRs. The values in the box show the median methylation index of the DMRs. Due to the impossibility of haplotype phasing, the underlined values reflect the methylation index calculated from total reads. The blue background indicates hypomethylated DMRs, the red background indicates hypermethylated DMRs, the light blue background indicates + 3SD of the control, and the light red background indicates – 3SD of the control. DMR, differentially methylated region; methylation array, array-based methylation analysis using the Infinium MethylationEPIC Kit (EPIC) (Illumina); SD, standard deviation; Pt.1, multi-locus imprinting disturbance patient with *ZNF445* variant; Pt. 2, multi-locus imprinting disturbance patient with *NLRP2* variant

We obtained median coverage of all target regions exceeding 25 in all controls except for regions of *NLRP2*, *NLPR7*, and *ZFP57* genes (Additional file 1: Table S1). The previous reports suggested that coverage of 12 or more reads for SVs, 6 or more reads for homozygous variants, and 8 or more for heterozygous variants is required to obtain reliable sequencing results in LRS [36, 37]. Regarding the *H19*-DMR, we first had no aligned reads and obtained the reads aligned for this DMR after excluding the chr11_KI270721v1_random from the reference fasta file (GRCh38). Consistent with this, it has been reported that the *H19*-DMR had a low coverage [35, 38] and conversion of the reference file from GRCh38 to T2T-CHM13 increased the coverage of the *H19*-DMR [38]. To obtain sufficient reads, paying attention to the reference for the *H19*-DMR is necessary. Determining the minimum coverage for methylation analysis using LRS has not reached a consensus. A previous study suggested that coverage for methylation analysis in LRS requires 10 or more reads for calculating MIs, in accordance with the standard coverage in WGBS [39]. Based on this report, we used only data with coverage of 10 or more for each CpG per allele in controls and calculated the normal methylation range (Table 3 and Additional file 3: Table S3). As shown in Fig. 3, which demonstrates the results of duplicated T-LRS in identical controls, the MIs showed high reproducibility even when different types of flow cells were used in repeated experiments. However, considering the coverage of approximately 10 to 100, it would be challenging to distinguish MI differences at the third decimal place accurately; therefore, we applied MI to two decimal places.

The T-LRS analysis using our system with a single PromethION flow cell in Patients 1 and 2 with MLID confirmed pathogenic variants of *ZNF445* on both alleles in Patient 1 with 132.9 median coverage and that of *NLRP2* on the maternal allele in Patient 2 with 11.5 median coverage (Additional file 7: Table S6). Our study also showed that methylation defect patterns in Patients 1 and 2 were similar to those detected by array-based methylation analysis using EPIC, although T-LRS identified more abnormally methylated DMRs using EPIC (Fig. 4). Differences in the number of control samples (T-LRS vs. EPIC: 6 vs. 16) and the criteria for normal range (minimum to maximum of normal controls vs. $|MMI| > 3$) may lead to a higher number of abnormally methylated DMRs in T-LRS. Furthermore, in nine cases with suspected IDs,

T-LRS identified methylation defects, deletions, and loss of heterozygosity leading to (epi)genetic diagnosis. T-LRS identified the loss of heterozygosity in Case 1 with KOS and the *STX16* deletion detected in Case 2 with PHP1B. The MS-MLPA Probe-mix ME034, used for screening tests for IDs, cannot detect these molecular abnormalities. As a point to note, we found that CpGs, which were unable to undergo haplotype phasing correctly, had values slightly exceeding the standard range defined as from the minimum to the maximum of normal controls. These results highlight the utility of methylation analysis using T-LRS and indicate the need for caution in interpreting methylation analysis results for DMRs that cannot undergo haplotype phasing.

The definition of the normal range of each CpG in the DMRs revealed that methylation patterns are different among DMRs. In most DMRs, CpGs at the beginning and end of the DMR were incompletely differentially methylated, and in some DMRs, such as the *MEG3*:TSS-DMR, *H19*-DMR, and *GNAS-AS1*:TSS-DMR, the region with completely differentially methylated CpGs and the region with incompletely differentially methylated CpGs were mixed (Fig. 2 and Additional file 5: Table S4). Because the regions with completely differentially methylated CpGs have a possibility to include the critical sequences for establishing or maintaining DNA methylation, such as the transcription factor binding site, clarification of detailed methylation levels of CpGs in the DMRs on each parental allele provides important information for elucidating the regulatory mechanism in the imprinted regions. As shown in Table 5, our T-LRS system evaluated more CpGs than pyrosequencing, MS-MLPA, and array-based methylation analysis using EPIC. In addition, our T-LRS system showed that CpGs evaluated by EPIC in the CA-DMRs were not completely differentially methylated on each parental allele (Additional file 5: Table S4). These findings suggest that interpretation using EPIC data for the DMR requires attention to the probes' location in the EPIC array. The CA-DMRs other than the *IGF2*:Ex9-DMR, *IGF2*:alt-TSS-DMR, and *MEG3/DLK1*:IG-DMR were classified as Complete-DMRs (Table 2 and Table 4) having large differences in MIs of CpGs in the DMRs between maternal and paternal alleles, and CpGs in the CA-DMR examined by conventionally targeted methylation analysis had large ΔMIs. It is reasonable that methylation analysis, such as MS-MLPA targeting CA-DMRs, as first-line genetic testing for IDs be recommended.

In this study, the number of reads with methylation information for CpGs was 50–80% of the coverage, calculated using Samtools depth. We used Modkit to classify haplotypes based on SNPs and indels. In this study, we set the input DNA length to 10–15 kb; therefore, the absence of SNPs or indels within 10 kb from the 5′-end and 3′-end of the DMR produces the reads classified into the "unphased" for haplotype classification by Modkit. As a result, the number of reads with methylation information classified as haplotype 1 or 2 was reduced. A longer setting for the length of the input DNA may improve the coverage, but the longer input DNA length results in a clog of the pores due to the characteristics of the adaptive sampling, in which off-target strands are ejected, and sequencing efficiency decreases. On the other hand, lowering the methylation probability in Modkit increases the number of reads with methylation information, but this reduces the accuracy of the methylation or non-methylation calls. Further improvement of the adaptive sampling system and fine-tuning for the methylation probability in Modkit should increase the reads with methylation information.

Due to clinical overlap among IDs and MLID involving various loci, genetic testing targeting a single ID may not always yield a definitive diagnosis of ID. Moreover, multiple analyses are often required to identify the etiology in cases with IDs that exhibit atypical methylation defect patterns. In this context, T-LRS identifies the etiologies more efficiently than conventional analysis methods, which combine various analytical techniques. In addition, T-LRS can easily add new ID-responsible genes or regions to the target region. However, at present, the cost of T-LRS analysis is notably higher than that of conventional methods; for example, a single T-LRS analysis costs approximately $1600, whereas EPIC costs $300, MS-MLPA $160, and array-based comparative genomic hybridization $300–$600 in Japan. Considering its cost, T-LRS is currently not the first choice for genetic testing in cases with suspected typical IDs. Cost reduction for T-LRS and an increased number of reads with methylation information through technological innovation should make T-LRS a mainstream analysis method for IDs.

Conclusions

We established a T-LRS system targeting all ID-related regions, defined a normal range of MIs in CpGs in the DMRs on each parental allele, and demonstrated the reliability of structural and methylation analyses using T-LRS in patients with MLID. T-LRS is a valuable tool for efficient genetic diagnosis in patients with IDs and contributes to elucidating the regulatory mechanisms in the imprinted regions.

Abbreviations

C	Unmethylated cytosine
CA	Clinically associated
DMR	Differentially methylated region
EPIC	Array-based methylation analysis using the Infinium MethylationEPIC Kit (Illumina)
Ex	Exon

H19	H19/IGF2:IG
ID	Imprinting disorder
IG	Intergenic
IGV	Integrative Genomics Viewer
Int	Intron
KOS	Kagami-Ogata syndrome
LRS	Long-read sequencing
MLID	Multi-locus imprinting disturbance
MI	Methylation index
MMI	Median MI
MS-MLPA	Methylation-specific multiple ligation-dependent probe amplification
NC	Non-clinical
ONT	Oxford Nanopore Technologies
PHP1B	Pseudohypoparathyroidism type 1B
SCMC	Subcortical maternal complex
SD	Standard deviation
SNP	Single-nucleotide polymorphism
SNV	Single-nucleotide variant
SRS	Silver-Russell syndrome
SV	Structural variants
T-LRS	Targeted LRS
TSS	Transcription start site
TS14	Temple syndrome
UPD	Uniparental disomy
WGBS	Whole genome bisulfite sequencing
5mC	5-Methylcytosine

Supplementary Information

The online version contains supplementary material available at https://doi.org/10.1186/s13073-025-01559-w.

Additional file 1. Table S1. Targeted regions and mean coverage in the controls.

Additional file 2. Table S2. Clinical manifestations in nine cases with suspected imprinting disorders.

Additional file 3. Table S3. Raw data of methylation analysis for the differentially methylated regions (DMRs). A: Details of methylation information in Complete-DMRs and Partial-DMRs. B: Details of methylation information in Non-DMRs. C: Methylation index of DMRs classified by a phasing error. D: Methylation index of each CpG in the paternal allele. E: Methylation index of each CpG in the maternal allele. F: Raw data.

Additional file 4. Fig. S1. The normal range of methylation index of CpGs in the MKRN3:transcription start site-differentially methylated region. Fig. S2. Integrative genomics viewer screen capture images in a homozygous variant of ZNF445 on Patient 1 and a heterozygous variant of NLRP2 on Patient 2. Fig. S3-11. The results of (epi)genetic analyses for Cases 1–9.

Additional file 5. Table S4. Methylation index of each CpG in the clinically associated differentially methylated regions.

Additional file 6. Table S5. Raw data of validation analysis for the differentially methylated regions (DMRs).

Additional file 7. Table S6. Raw data for long-read sequencing of patients with multi-locus imprinting disturbance.

Additional file 8. Table S7. Raw data for long-read sequencing of nine cases with suspected imprinting disorders. A: Summary of methylation information in nine cases. B-J: Raw data of Cases 1–9.

Acknowledgements
We are grateful to all controls and patients for their cooperation. We thank Dr. Tomoe Ogawa and Ms. Aki Ueda for their support in molecular and data analysis.

Authors' contributions
TU performed the molecular and data analyses, designed and created the project, and wrote the paper. HM, MI, SN, and K-HI performed the molecular and data analyses. AH, YO, KI, H-OK, HK, YK, and KN designed and created the project. MF reviewed the paper and supervised the project. MK designed the project, performed the molecular analysis, wrote the paper, and gave the final approval of the version to be published. All authors read and approved the final manuscript.

Funding
This work was supported by grants from the National Center for Child Health and Development (2022B-5), the Japan Society for the Promotion of Science (JSPS) (22K07858 [C]), the Japan Agency for Medical Research and Development (AMED) (JP25ek0109805), the Japanese Society for Pediatric Endocrinology Future Development Grant supported by Novo Nordisk Pharma Ltd., the NOVARTIS Foundation (Japan), and Kawano Masanori Memorial Public Interest Incorporated Foundation for Promotion of Pediatrics.

Data availability
The datasets supporting the conclusions of this article are included within the article and its additional files.

Declarations

Ethics approval and consent to participate
This study was approved by the Institutional Review Board Committee of the National Center for Child Health and Development (permit No. 518 and 2024–245) and complied with the Declaration of Helsinki. We obtained written informed consent from all individuals or their parents to participate in this study.

Consent for publication
We obtained written informed consent from the individuals and the patients or the patients' parents to publish the individuals' molecular information and patients' clinical and molecular information, respectively.

Competing interests
The authors declare no competing interests.

Author details
[1]Department of Molecular Endocrinology, National Research Institute for Child Health and Development, 2-10-1 Okura, Setagaya-Ku, Tokyo 157-8535, Japan. [2]Department of Pediatrics, Nagasaki University Graduate School of Biomedical Sciences, 1-7-1 Sakamoto, Nagasaki 852-8102, Japan. [3]Division of Diversity Research, National Research Institute for Child Health and Development, 2-10-1 Okura, Setagaya-Ku, Tokyo 157-8535, Japan. [4]Center for Postgraduate Education and Training, National Center for Child Health and Development, 2-10-1 Okura, Setagaya-Ku, Tokyo 157-8535, Japan. [5]Department of Maternal-Fetal Biology, National Research Institute for Child Health and Development, 2-10-1 Okura, Setagaya-Ku, Tokyo 157-8535, Japan. [6]Department of Genome Medicine, National Center for Child Health and Development, 2-10-1 Okura, Setagaya-Ku, Tokyo 157-8535, Japan. [7]Division of Collaborative Research, National Center for Child Health and Development, 2-10-1 Okura, Setagaya-Ku, Tokyo 157-8535, Japan.

Received: 2 May 2025 Accepted: 6 October 2025
Published online: 18 November 2025

References

1. Monk D, Mackay DJ, Eggermann T, Maher ER, Riccio A. Genomic imprinting disorders: lessons on how genome, epigenome and environment interact. Nat Rev Genet. 2019;20(4):235–48. https://doi.org/10.1038/s41576-018-0092-0.
2. Eggermann T, et al. Imprinting disorders. Nat Rev Dis Primers. 2023;9(1):33. https://doi.org/10.1038/s41572-023-00443-4.
3. Monk D, Sanchez-Delgado M, Fisher R. NLRPs, the subcortical maternal complex and genomic imprinting. Reproduction. 2017;154(6):R161–70. https://doi.org/10.1530/REP-17-0465.
4. Eggermann T, et al. The maternal uniparental disomy of chromosome 6 (upd(6)mat) "phenotype": result of placental trisomy 6 mosaicism? Mol Genet Genomic Med. 2017;5(6):668–77. https://doi.org/10.1002/mgg3.324.

5. Nakamura A, et al. A case of paternal uniparental isodisomy for chromosome 7 associated with overgrowth. J Med Genet. 2018;55(8):567–70. https://doi.org/10.1136/jmedgenet-2017-104986.
6. Inoue T, et al. Molecular and clinical analyses of two patients with UPD(16)mat detected by screening 94 patients with Silver-Russell syndrome phenotype of unknown aetiology. J Med Genet. 2019;56(6):413–8. https://doi.org/10.1136/jmedgenet-2018-105463.
7. Mackay DJ, et al. Multi-locus imprinting disturbance (MLID): interim joint statement for clinical and molecular diagnosis. Clin Epigenetics. 2024;16(1):99. https://doi.org/10.1186/s13148-024-01713-y.
8. Kagami M, et al. ZNF445: a homozygous truncating variant in a patient with Temple syndrome and multilocus imprinting disturbance. Clin Epigenetics. 2021;13(1):119. https://doi.org/10.1186/s13148-021-01106-5.
9. Laszlo AH, et al. Detection and mapping of 5-methylcytosine and 5-hydroxymethylcytosine with nanopore MspA. Proc Natl Acad Sci U S A. 2013;110(47):18904–9. https://doi.org/10.1073/pnas.1310240110.
10. Schreiber J, Karplus K. Analysis of nanopore data using hidden Markov models. Bioinformatics. 2015;31(12):1897–903. https://doi.org/10.1093/bioinformatics/btv046.
11. Shafin K, et al. Haplotype-aware variant calling with PEPPER-Margin-DeepVariant enables high accuracy in nanopore long-reads. Nat Methods. 2021;18(11):1322–32. https://doi.org/10.1038/s41592-021-01299-w.
12. Loose M, Malla S, Stout M. Real-time selective sequencing using nanopore technology. Nat Methods. 2016;13(9):751–4. https://doi.org/10.1038/nmeth.3930.
13. Payne A, Holmes N, Clarke T, Munro R, Debebe BJ, Loose M. Readfish enables targeted nanopore sequencing of gigabase-sized genomes. Nat Biotechnol. 2021;39(4):442–50. https://doi.org/10.1038/s41587-020-00746-x.
14. Yamada M, et al. Diagnosis of Prader-Willi syndrome and Angelman syndrome by targeted nanopore long-read sequencing. Eur J Med Genet. 2023;66(2):104690. https://doi.org/10.1038/s41587-020-00746-x.
15. Holthöfer L, et al. A case of an Angelman-syndrome caused by an intragenic duplication of *UBE3A* uncovered by adaptive nanopore sequencing. Clin Epigenetics. 2024;16(1):101. https://doi.org/10.1186/s13148-024-01711-0.
16. Miller DE, et al. Targeted long-read sequencing identifies a retrotransposon insertion as a cause of altered GNAS exon A/B methylation in a family with autosomal dominant pseudohypoparathyroidism type 1b (PHP1B). J Bone Miner Res. 2022;37(9):1711–9. https://doi.org/10.1002/jbmr.4647.
17. Kilich G, et al. Kagami Ogata syndrome: a small deletion refines critical region for imprinting. NPJ Genom Med. 2024;9:5. https://doi.org/10.1038/s41525-023-00389-2.
18. Carvalho CM, et al. Interchromosomal template-switching as a novel molecular mechanism for imprinting perturbations associated with Temple syndrome. Genome Med. 2019;11:25. https://doi.org/10.1186/s13073-019-0633-y.
19. Kraft F, Wesseler K, Begemann M, Kurth I, Elbracht M, Eggermann T. Novel familial distal imprinting centre 1 (11p15.5) deletion provides further insights in imprinting regulation. Clin Epigenetics. 2019;11(1):30. https://doi.org/10.1186/s13148-019-0629-x.
20. Monk D, et al. Recommendations for a nomenclature system for reporting methylation aberrations in imprinted domains. Epigenetics. 2018;13(2):117–21. https://doi.org/10.1080/15592294.2016.1264561.
21. Joshi RS, et al. DNA methylation profiling of uniparental disomy subjects provides a map of parental epigenetic bias in the human genome. Am J Hum Genet. 2016;99(3):555–66. https://doi.org/10.1016/j.ajhg.2016.06.032.
22. Urakawa T, et al. Comprehensive molecular and clinical findings in 29 patients with multi-locus imprinting disturbance. Clin Epigenetics. 2024;16(1):138. https://doi.org/10.1186/s13148-024-01744-5.
23. Mantovani G, et al. Diagnosis and management of pseudohypoparathyroidism and related disorders: first international consensus statement. Nat Rev Endocrinol. 2018;14(8):476–500. https://doi.org/10.1038/s41574-018-0042-0.
24. Wakeling EL, et al. Diagnosis and management of Silver-Russell syndrome: first international consensus statement. Nat Rev Endocrinol. 2017;13(2):105–24. https://doi.org/10.1038/nrendo.2016.138.
25. Kagami M, Kurosawa K, Miyazaki O, Ishino F, Matsuoka K, Ogata T. Comprehensive clinical studies in 34 patients with molecularly defined UPD(14)pat and related conditions (Kagami-Ogata syndrome). Eur J Hum Genet. 2015;23(11):1488–98. https://doi.org/10.1038/ejhg.2015.13.
26. Oxford Nanopore Technologies. Guppy basecalling software. https://community.nanoporetech.com/ (No longer available).
27. Oxford Nanopore Technologies. Dorado basecalling model v4.3. https://github.com/nanoporetech/dorado (Accessed 6 Oct 2025).
28. Illumina, Inc. Homo_sapiens_NCBI_GRCh38Decoy. iGenomes (Illumina). https://s3.amazonaws.com/igenomes.illumina.com/Homo_sapiens/NCBI/GRCh38Decoy/Homo_sapiens_NCBI_GRCh38Decoy.tar.gz (Accessed 6 Oct 2025).
29. Li H. Minimap2: pairwise alignment for nucleotide sequences. Bioinformatics. 2018;34(18):3094–100. https://doi.org/10.1093/bioinformatics/bty191.
30. Robinson JT, et al. Integrative genomics viewer. 2011;29(1):24–6. https://doi.org/10.1038/nbt.1754.
31. Danecek P, et al. Twelve years of SAMtools and BCFtools. Gigascience. 2021;10(2):giab008. https://doi.org/10.1093/gigascience/giab008.
32. Oxford Nanopore Technologies. modkit. Github. https://github.com/nanoporetech/modkit (Accessed 6 Oct 2025).
33. Bilo L, et al. Molecular characterisation of 36 multilocus imprinting disturbance (MLID) patients: a comprehensive approach. Clin Epigenetics. 2023;15(1):35. https://doi.org/10.1186/s13148-023-01453-5.
34. Fuke T, et al. Molecular and clinical studies in 138 Japanese patients with Silver-Russell syndrome. PLoS ONE. 2013;8(3):e60105. https://doi.org/10.1371/journal.pone.0060105.
35. Geysens M, et al. Clinical evaluation of long-read sequencing-based episignature detection in developmental disorders. Genome Med. 2025;17(1):1. https://doi.org/10.1186/s13073-024-01419-z.
36. Harvey WT, et al. Whole-genome long-read sequencing down sampling and its effect on variant calling precision and recall. Genome Res. 2023;33(12):2029–40. https://doi.org/10.1101/gr.278070.123.
37. Mahmoud M, et al. Utility of long-read sequencing for all of us. Nat Commun. 2024;15(1):837. https://doi.org/10.1038/s41467-024-44804-3.
38. Bækgaard CH, Lester EB, Møller-Larsen S, Lauridsen MF, Larsen MJ. Nanoimprint: a DNA methylation tool for clinical interpretation and diagnosis of common imprinting disorders using nanopore long-read sequencing. Ann Hum Genet. 2024;88(5):392–8. https://doi.org/10.1111/ahg.12556.
39. Sigurpalsdottir BD, et al. A comparison of methods for detecting DNA methylation from long-read sequencing of human genomes. Genome Biol. 2024;25(1):69. https://doi.org/10.1186/s13059-024-03207-9.

Publisher's Note